

A first step in the nuclear inverse Kohn-Sham problem: from densities to potentials

G. Accorto, P. Brandolini, F. Marino, A. Porro, and A. Scalesi

Dipartimento di Fisica “Aldo Pontremoli”, Università degli Studi di Milano, Via Celoria 16, 20133 Milano, Italy

G. Colò* and X. Roca-Maza†

Dipartimento di Fisica “Aldo Pontremoli”, Università degli Studi di Milano, Via Celoria 16, 20133 Milano, Italy and INFN, Sezione di Milano, Via Celoria 16, 20133 Milano, Italy

E. Vigezzi‡

INFN, Sezione di Milano, Via Celoria 16, 20133 Milano, Italy

(Dated: October 27, 2022)

Nuclear Density Functional Theory (DFT) plays a prominent role in the understanding of nuclear structure, being the approach with the widest range of applications. Hohenberg and Kohn theorems warrant the existence of a nuclear Energy Density Functional (EDF), yet its form is unknown. Current efforts to build a nuclear EDF are hindered by the lack of a strategy for systematic improvement. In this context, alternative approaches should be pursued and, so far, an unexplored avenue is that related to the inverse DFT problem. DFT is based on the one-to-one correspondence between Kohn-Sham (KS) potentials and densities. The exact EDF produces the exact density, so that from the knowledge of experimental or *ab initio* densities one may deduce useful information through reverse engineering. The idea has already been proven to be useful in the case of electronic systems. The general problem should be dealt with in steps, and the objective of the present work is to focus on testing algorithms to extract the Kohn-Sham potential within the simplest ansatz from the knowledge of the experimental neutron and proton densities. We conclude that while robust algorithms exist, the experimental densities bring in some critical aspect.

PACS numbers: 21.60.Jz

I. INTRODUCTION

Density Functional Theory (DFT) has become gradually one of the best tools of choice for the study of nuclear structure [1, 2], trying to follow the path that led to the success of electronic DFT [3, 4]. There are analogies and differences between the two cases. One can expect that building an Energy Density Functional (EDF) for nuclei is harder than doing the same for electronic systems, in keeping with the more involved, and less well known, underlying nucleon-nucleon (NN) interaction. This interaction is strongly spin- and isospin-dependent, while momentum-dependent, spin-orbit and tensor terms are far from being negligible and there are also three-body (NNN) components — all this is at variance with the Coulomb case.

DFT is grounded in the Hohenberg-Kohn Theorems (HKTs), stating that a universal EDF must exist and yet do not provide any guidance on how to build its terms [5]. The most used and well-established nuclear EDFs like the Skyrme and Gogny ones (we do not discuss covariant functionals which, though very successful, are outside our scope here) include terms that have their origin in central two-body forces and have a form proportional to the square of the total number density (ρ^2),

repulsive terms which depend on a larger power of ρ to mimic short-range repulsion, besides the terms that have been mentioned in the previous paragraph and account for spin forces, spin-orbit forces etc. They contain parameters that are fitted on experimental properties of selected nuclei, can be dubbed as phenomenological and lack from the beginning a clear mechanism for systematic improvement.

Recently, several groups have undertaken important steps to build more general EDFs, in which one starts from ρ -dependent terms, and include other terms that depend on gradients $\vec{\nabla}\rho$ up to a given order (see [6], as well as [7] and references therein). The systematic construction of all possible densities and their gradients has been described in the past [8, 9], together with the systematic classification of all possible terms that should enter a nuclear EDF [10]. These terms are all the scalar quantities that can be built out of densities and that are invariant under parity, time-reversal, rotational, translational and isospin transformations. As obvious, the number of such terms can be very large and fitting too general EDFs may become either technically prohibitive, or unpractical due to the lack of experimental input, or both.

Other attempts have been made to derive the nuclear EDFs from fundamental approaches. On this regard, general ideas and perspectives can be found in Ref. [11]. Whereas in Refs. [12–14] attempts have been made to derive non-relativistic EDFs from Brückner-Hartree-Fock calculations in uniform matter, a hybrid approach has been followed in Refs. [15–17], in which the long-range, pion exchange-like part of the EDF has been derived from

* gianluca.colo@mi.infn.it

† xavier.roca.maza@mi.infn.it

‡ enrico.vigezzi@mi.infn.it

chiral forces and short-range coupling constants are left to be fitted against phenomenological data. While trying to derive EDFs from *ab initio* theories, or to generalize their structure, may produce some breakthroughs, perhaps new mathematical or computational techniques are also worth attempting.

The present work is based on the Kohn-Sham (KS) realization of the HKTs [18]. We define as direct problem the one in which, given a KS functional and the associated effective potential, we deduce the density that can be compared to experiment together with the total ground-state energy. We define as inverse problem the one in which starting from a given (supposedly exact) density, we deduce the effective KS potential. Solving the inverse problem is obviously appealing as it can constrain the phenomenological KS potential and the phenomenological EDF at his basis. In the case of electronic systems there have been several attempts to attack the inverse KS problem. In this work, we closely follow some of the inversion methods reviewed in Ref. [19], in which some basic concepts and techniques are discussed in detail. Hence, the current work is motivated by the idea that if the density is the basic variable to describe fermionic systems, as guaranteed by the HKTs, the measured nuclear densities should contain, in principle, all the relevant information to constrain the nuclear EDF.

Before presenting the KS ansatz and its inverse formulation, two important points need to be clarified.

Intrinsic density. A fundamental difference between DFT in finite electronic systems and nuclei consists in the fact that in the former case the fixed ion positions constrain the shape of the system in the laboratory frame. In nuclei, that are self-bound systems, this is not the case. The usual HK theorem, as it has been argued by several authors [20], is formulated for the laboratory density, while experiments on nuclei probe the intrinsic density (relative to the nuclear center of mass). Nonetheless, it has been proven that, given an arbitrary Hermitian operator \hat{Q} , one can build an energy functional depending on $Q(\vec{r}) \equiv \langle \hat{Q}(\vec{r}) \rangle$ that is universal in the HK sense and has its minimum at the correct value of Q with the correct energy (see [21] and references therein). In this respect, one can replace the laboratory density with the intrinsic density in the HK theorem [20, 22, 23].

Nuclear densities. In the nuclear case different type of densities exist: total number density, spin- and isospin-densities, spin-orbit densities, etc. As a first step, in the present contribution, we employ neutron and proton number densities alone. If, and how, the inverse KS problem can be formulated in terms of all relevant nuclear densities and gradients of such densities and deduce a more appropriate form for the effective KS potential, is left for future studies.

The structure of the present paper is as follows. In Sec. II, we briefly introduce the KS realization of the HKTs as well as the inverse problem. In Sec. III, we describe the two adopted computational approaches. In Sec. IV, we test the numerical methods presented in

Sec. III by using theoretical densities generated from a mean-field approach. In Sec. V, we deduce from experiment the KS potential for protons in ^{40}Ca , and for neutrons and protons for ^{208}Pb . Conclusions will be presented in Sec. VI.

II. INVERSE KOHN-SHAM PROBLEM

Our general framework is now well defined. Hence, by assuming the KS ansatz, one has a practical way to build EDFs. The main point of the KS ansatz consists in assuming that the neutron or proton number density¹ can be expressed as the sum over a number N_{orb} of KS single-particle orbitals ϕ_i , namely

$$\rho(\vec{r}) = \sum_i^{N_{orb}} |\phi_i(\vec{r})|^2. \quad (1)$$

In addition, the kinetic energy T is taken with the same form as in the independent particle case (i.e. uncorrelated). Then, the EDF turns out to be of the form

$$E[\rho] = \sum_i \int d^3r \phi_i^*(\vec{r}) \left(-\frac{\hbar^2}{2m} \nabla^2 \phi_i(\vec{r}) + F[\rho] \right), \quad (2)$$

and its minimization leads to the well-known Kohn-Sham equations of the type

$$\left(-\frac{\hbar^2}{2m} \nabla^2 + \frac{\delta F[\rho]}{\delta \rho} \right) \phi_i(\vec{r}) = \varepsilon_i \phi_i(\vec{r}), \quad (3)$$

where ε_i are the so-called Kohn-Sham eigenvalues. The quantity $\frac{\delta F[\rho]}{\delta \rho}$ plays the role of an effective potential and will be hereafter denoted by $U[\rho]$. If F is assumed, U is given and the density can be found. In this context, the IKS problem consists in reversing the procedure and deriving the effective potential $U[\rho]$ given the knowledge of ρ . In the present work ρ will represent the neutron and proton densities alone. That is, we will assume that the KS potential is a function of only the spatial coordinates. This potential is determined except for a constant shift.

To the best of our knowledge, this is the first attempt to address the IKS problem in the nuclear case. In the literature, one finds several formulations of the IKS problem for the case of electronic systems, (see e.g. Ref. [24] for early references). The two approaches that we discuss below have been originally introduced in Refs. [25] and [19]. The IKS problem has been solved in the case of the He atom, where an exact analytic solution for wave functions and densities is available [26], and this has allowed testing various approximate methods [27]. Among recent papers, we also would like to mention Refs. [28, 29], that deal with the time-dependent inverse problem, and

¹ From here on, we will refer to number density as density.

Ref. [30], that shows the connection between different IKS strategies. This list is not meant to be exhaustive.

In the following we discuss some more specific issues that are important for a better understanding of the IKS problem.

Ill-posed problem. One finds ample discussion in the literature, regarding the question whether the IKS is well-posed, according to the definition given by J. Hadamard [31], or not. We miss a formal proof of the fact that IKS is well-posed, except for the case of discretized systems [32], but this does not mean that the IKS problem is necessarily ill-posed. Still, its numerical solution is a very delicate matter. From a theoretical point of view, the existence of a Kohn-Sham potential for a given experimental density is not guaranteed, although the uniqueness of the solution is guaranteed if a method converges (see, e.g., the discussion of not v -representable densities in [33]). Furthermore, errors and missing information in the experimental data can lead to violations of the Hadamard conditions. We have selected two of the algorithms introduced in [19] and references therein, and applied them to the nuclear case for the first time. Some of the pathologies inherent to experimental nuclear densities will be discussed in Sec. V.

Nuclear densities. As already stressed, realistic EDFs do not simply depend on the total density but on gradients, spin- and isospin-densities, spin-orbit densities etc. Our inversion of Eq. (3) is intended as a first step towards more realistic applications. Still, it is interesting to investigate which are the limitations of our assumption, if any, when starting not from previous knowledge of realistic nuclear EDFs, but rather from the *experimental densities*. In other words, we try to determine the information contained in the experimental densities about the effective potential $U[\rho(\vec{r})]$, without any prejudice but those inherent in the experimental analysis.

EDF from KS potential. Going one step back from the effective potential $U[\rho(\vec{r})]$ to the functional $F[\rho(\vec{r})]$ is much harder. $U[\rho(\vec{r})]$ is determined aside from an arbitrary constant shift. In addition, we cannot dispose of densities and potentials for systems very close to a given one, so to imagine a functional integration; whether this can be possible using *ab initio* techniques and/or whether this idea is related to the one introduced in Ref. [34], is left for future studies.

III. INVERSE KOHN-SHAM PROBLEM: TWO DIFFERENT METHODS

We use two different methods to extract the KS potential $U[\rho]$ from the neutron and proton densities. We start from Eq. (3) and assume that the effective potential $U[\rho]$ is only position-dependent in keeping with the KS ansatz described in Sec. II. Thus, within this ansatz, non-local effects and the spin-orbit potential are not explicitly taken into account. The latter approximation should not impact much on the KS potential since spin-

orbit effects are not expected to markedly change the KS orbitals. Consequently, from Eq. (1), the density should be almost untouched. Non-locality could be accounted via gradients of the density, we leave this for future improvements. Among others, the main effect of this approximation is to prevent the appearance of neutron and proton effective masses. As for Coulomb interaction between protons, we implicitly assume a local form within $U[\rho]$ in Eq. (3). This is known to work well for the description of the total binding energy and density in nuclei.

Among the two methods, the first we shall present is based on an iterative procedure and was introduced by R. Van Leeuwen and E.J. Baerends [25]: it will be called vLB method. The other method consists instead in the constrained minimization of the kinetic energy T , in the spirit of KS that introduce an auxiliary system of independent particles with the same density of the system under study: this method will be called constrained variational, or CV, method. In choosing the notation vLB and CV, we closely follow Ref. [19]. In both cases we will use $\tilde{\rho}$ to denote the target density. That is, the density to be reproduced. We will restrict ourselves to doubly-magic, spherical systems.

A. The vLB method

The aim of this procedure is to bring the calculated density as close as possible to the given target density by iteration. That is, by starting from an initial guess of $U[\rho]$, implement the vLB iterative algorithm [25] and repeat until $U[\rho]$ is stable. The derivation of the vLB algorithm is very simple so we briefly describe it in what follows.

Let us start by writing the direct formulation of the KS equation (3) in spherical symmetry,

$$\left[-\frac{\hbar^2}{2m} \frac{d^2}{dr^2} + \frac{\hbar^2 l(l+1)}{2mr^2} + U(r) \right] u_i(r) = \varepsilon_i u_i(r), \quad (4)$$

where $u_i(r)$ are the reduced radial wave functions and $U(r) \equiv U[\rho(r)]$ is the effective Kohn-Sham potential that has been already introduced. The simplifications that lead to a simple dependence on r have been also discussed. In the case of spherical nuclei, i stands for n, l, j which denote the principal quantum number, the orbital angular momentum and the total angular momentum. The full wave function reads $\phi_i(\vec{r}) \equiv \frac{u_{nlj}(r)}{r} [Y_l(\theta, \phi) \otimes \chi_{1/2}]_{jm}$, where m denotes the projection of the angular momentum on the z -axis. We do not use specific notations for protons and neutrons as the iterative procedure is carried out independently for the two species. As already stressed, we assume here that the spin-orbit potential does not change significantly the shape of the radial wave function, so that $u_i(r)$ is effectively the same for the spin-orbit partners $j = l + 1/2$ and $j = l - 1/2$.

The boundary conditions at the origin associated with Eq. (4) are well known,

$$\lim_{r \rightarrow 0} u(r) = r^{l+1}, \quad (5a)$$

$$\lim_{r \rightarrow 0} u'(r) = (l+1)r^l, \quad (5b)$$

and these allow to solve the *direct* Kohn-Sham equation (4) by means of a shooting algorithm. Thus, we find the energy eigenvalues and the eigenfunctions and derive the density $\rho(r)$ as

$$\rho(r) = \frac{1}{4\pi r^2} \sum_{i=0}^{N_{\text{orb}}} n_i u_i^2(r), \quad (6)$$

where n_i is the occupation factor of the orbital i . In principle, n_i could be taken as a fractional particle number (cf. Ref. [35]). However, we assume here $n_i = 2j + 1$ since we limit ourselves to closed shell nuclei. We have checked that, not having implemented any spin-orbit effect in Eq. (4), working within the uncoupled l and s or coupled $j = l + s$ schemes provide identical results.

The vLB inverse algorithm [25] as well as a slightly different algorithm [24] not discussed here can be obtained by algebraic manipulation of Eq. (4). Specifically, multiplying Eq.(4) by $n_i u_i(r)$ at both sides, summing over i and dividing by $4\pi r^2 \rho(r)$, one finds

$$U(r) = \frac{1}{4\pi r^2 \rho(r)} \sum_{i=0}^{N_{\text{orb}}} \left[n_i u_i(r) \left(\frac{\hbar^2}{2m} \frac{d^2}{dr^2} - U_l \right) u_i + \varepsilon_i n_i u_i^2 \right], \quad (7)$$

where U_l is a shorthand notation for the centrifugal potential. Now we need to define the iterative process from that equation. Denoting iteration numbers by superscripts, a guess for the new potential $U^{(k+1)}$ can be obtained substituting ρ with $\tilde{\rho}(r)$ in the denominator in r.h.s. of Eq. (7) and realizing that the rest of the r.h.s in the same equation correspond to the potential times the density determined in the previous iteration $4\pi r^2 \rho^{(k)}(r) U^{(k)}$. That is,

$$U^{(k+1)}(r) = \frac{1}{4\pi r^2 \tilde{\rho}(r)} \sum_{i=0}^{N_{\text{orb}}} \left[n_i u_i^{(k)}(r) \left(\frac{\hbar^2}{2m} \frac{d^2}{dr^2} - U_l \right) u_i^{(k)} + \varepsilon_i n_i \left(u_i^{(k)} \right)^2 \right] = \frac{\rho^{(k)}(r)}{\tilde{\rho}(r)} U^{(k)}(r). \quad (8)$$

Thus, the vLB inversion method consists in finding $u^{(k+1)}(r)$ from Eq. 4 assuming a starting potential $U^{k=1}(r)$, then calculate the density from Eq. (6), find the new potential by applying Eq. (8) and repeat until convergence. It is important to note that the iterative algorithm in Eq. (8) has a simple meaning. In regions where the density at the k -th step is larger than the target density the potential is increased in absolute value, and vice versa. This makes sense for repulsive potentials

as in the electronic case, but in the case of attractive potentials needed in nuclear physics, the opposite should happen. We then propose a modified algorithm:

$$U^{k+1}(r) = \begin{cases} \left(2 - \frac{n^k(r)}{\tilde{n}(r)} \right) U^k(r) & U^k(r) \leq 0 \\ \frac{n^k(r)}{\tilde{n}(r)} U^k(r) & U^k(r) > 0. \end{cases} \quad (9)$$

This algorithm works well in general but encounters numerical difficulties in the regions where the potential changes its sign. Therefore, we have preferred to add a constant to the potential so that it is always positive or negative in the region of interest. From a physical point of view, this shift does not affect the outcome of the calculations, because potentials are defined up to an arbitrary constant.

In practice, we have further modified the original algorithm (8). Replacing at each step $U^{(k)}$ directly with $U^{(k+1)}$ induces in some cases an oscillating behavior of the potential which prevents convergence, as is usual in iterative procedures. Therefore, in our case, at each iteration the new potential is built in a more conservative way, namely we perform the replacement

$$U^{(k+1)} \rightarrow \eta U^{(k+1)} + (1 - \eta) U^{(k)}, \quad (10)$$

with η as small as 0.01.

A simple alternative is to adopt the algorithm proposed in Eq. (16) of Ref. [19] (see also Ref. [24]). This algorithm is based on the very same idea of shifting the potential by a constant value γ , but with one modification. In brief, starting from Eq. (8),

$$U^{k+1}(r) + \gamma = \frac{\rho^{(k)}(r)}{\tilde{\rho}(r)} [U^{(k)}(r) + \gamma] \\ U^{k+1}(r) = \frac{\rho^{(k)}(r)}{\tilde{\rho}(r)} U^{(k)}(r) + \gamma \frac{\rho^{(k)}(r) - \tilde{\rho}(r)}{\tilde{\rho}(r)} \quad (11)$$

Now, the algorithm in Ref. [19] conveniently neglects the factor multiplying the potential $U^{(k)}(r)$ setting it to one. This allows one to avoid large changes in $U^{(k+1)}(r)$ as compared to the algorithm in Eq. (8). Indeed, with the algorithm [19],

$$U^{k+1}(r) = U^{(k)}(r) + \gamma \frac{\rho^{(k)}(r) - \tilde{\rho}(r)}{\tilde{\rho}(r)}, \quad (12)$$

changes can be controlled via the adopted value of γ . On top of that, the latter algorithm does not show any pathology related to the sign of the potential and, thus, provides a good numerical alternative. Interestingly, the algorithm in Eq. (12) is invariant under an arbitrary shift of the potential while the algorithms in Eqs. (8) and (9) are not.

We have checked that the presented algorithms produce compatible results within our numerical accuracy.

The convergence condition used to stop the iterative procedure is set in terms of the absolute variation of the potential, that is,

$$\max_r \left| U^{(k+1)}(r) - U^{(k)}(r) \right| < \alpha. \quad (13)$$

As already discussed, a starting guess $U^{(k=1)}(r)$ is needed in order to start the iterative procedure in Eqs.(9) or (12). However, it is remarkable that despite the simplicity of the inversion algorithms presented so far, the results we obtain are largely independent on the details of the starting potential. Actually, the algorithms have been proven to be robust enough so converge to the same results when assuming $U^{(k=1)}(r)$ to be a constant or the well known Woods-Saxon potential.

B. The CV method

In the CV method, the IKS problem is formulated as a variational problem. The formulation is in keeping with the KS method, that assert that for any interacting Fermi system one can always postulate an independent particle system with the same density. Accordingly, in the CV method one writes down the kinetic energy functional of the N fermions with the purpose of minimizing it. Therefore, in what follows, we shall use the name of objective functional for the expectation value of the kinetic energy associated with the wave function of N independent particles as in Eq. (2). The minimization is subject to the following constraints:

1. the single particle orbitals $\phi_i(\vec{r})$ must be orthonormal;

2. the density of the system $\rho(\vec{r})$ must reproduce the target density $\tilde{\rho}(\vec{r})$.

Let us start from the same assumptions as in the previous subsection. We assume we have N_{orb} single particle states and each of them has occupancy n_i . We prefer here to write the equation without going immediately to the spherically symmetric case, as the CV method is more apt for the generalization to the case in which this symmetry is totally or partially broken. The objective functional reads

$$T_s[\{\phi_i\}] = \sum_{i=1}^{N_{\text{orb}}} n_i \int d^3r \phi_i^*(\vec{r}) \left(-\frac{\hbar^2}{2m} \right) \nabla^2 \phi_i(\vec{r}). \quad (14)$$

The orthonormality of the orbitals is the first constraint and is expressed by

$$G_{ij}[\{\phi_i\}] = \int d^3r \phi_i^*(\vec{r}) \phi_j(\vec{r}) = \delta_{ij}, \quad (15)$$

while the equality of the density to the target density is the second constraint (see below). We introduce Lagrange multipliers that correspond to these constraints. Those associated with the constraints (15) are indicated as ε_{ij} , while we write the constraint associated with the density as $U(\vec{r})$. The constrained minimization of the objective functional is re-written as the free minimization of the functional that includes the Lagrange multipliers and it is named cost functional [36]. This cost functional reads

$$J[\{\phi_i\}; U(\vec{r}), \{\varepsilon_{ij}\}] = T_s[\{\phi_i\}] + \int d^3r U(\vec{r}) \rho(\vec{r}) - \sum_{i=1}^{N_{\text{orb}}} \sum_{j=1}^i \varepsilon_{ij} \int d^3r \phi_i^*(\vec{r}) \phi_j(\vec{r}). \quad (16)$$

Having written the cost functional, the CV method consists in solving

$$\delta J[\{\phi_i\}; U(\vec{r}), \{\varepsilon_{ij}\}] = 0. \quad (17)$$

Following Ref. [19], the variational equation (17) is transformed into a set of Schrödinger-like Euler-Lagrange equations. Since the wave functions ϕ_i are known from the optimization procedure for the cost functional (16), these Euler-Lagrange equations are now algebraic equations, whose unknowns are precisely $U(\vec{r})$ at each point of the grid and the Lagrange multipliers ε_{ij} associated with the orthonormality constraints.

In practical cases, the wave functions ϕ_i solution of the optimization of the cost functional are not perfectly orthonormal. Thus, the matrix ε_{ij} will not be exactly

diagonal. However, once diagonalized, ε_{ii} will provide the Kohn-Sham eigenvalues associated to the corresponding bases states. At the same time, the very form of Eq. (16) tells that the extracted Lagrange multiplier $U(\vec{r})$ is the Kohn-Sham potential. In this respect, the CV method is a direct formulation of the IKS.

Minimizing the cost functional $J[\{\phi_i\}; U(\vec{r}), \{\varepsilon_{ij}\}]$ means to find the set of orbitals ϕ_i , defined on a given domain, that gives the minimum value for the functional respecting the two constraints at the same time. Hence, an unrestricted three-dimensional formulation is technically involved. In order to compare to our results obtained with the vLB method presented in Sec. III A, we have limited ourselves to the case of spherical nuclei, as already discussed, so that the problem becomes one-dimensional,

namely the orbitals depend only on r . In spherical sym-

metry, Eq. (16) becomes

$$J[\{u_j\}; U(r), \{\epsilon_{ij}\}] = T_s[\{u_j\}] + 4\pi \int_0^\infty U(r)\rho(r)r^2 dr - \sum_{i=1}^{N_{orb}} \sum_{j=1}^i \epsilon_{ij} \delta_{l_i l_j} \delta_{j_i j_j} \int_0^\infty u_i(r)u_j(r) dr \quad (18)$$

The CV method has been implemented following some important modifications suggested in Ref. [19]. First, a new set of variables, *viz.* the re-scaled orbitals $f_i(r)$ that are defined by

$$u_i(r) = \sqrt{4\pi\tilde{\rho}(r)} r f_i(r), \quad (19)$$

have been introduced. The rationale behind this substitution is that we expect that $u_i^2(r) \approx 4\pi r^2 \tilde{\rho}(r)$, so that the re-scaling will produce new functions $f_i(r)$ of the order of ≈ 1 , characterized by a milder behavior as compared to $u_i(r)$. This helps in reducing the rounding errors that appear when operating with quantities of different orders of magnitude. The CV iterative procedure is started from a guess to the wave functions and not to the KS potential, at variance with the starting guess in the vLB procedure. Also in the case of the CV method, we have checked that the starting guess is not influencing the result of the minimization. Indeed, starting from constant wave functions or from harmonic oscillator orbitals ($\hbar\omega = 41A^{-1/3}$ MeV), we obtain satisfactory results.

The optimization of Eq. (17) is performed employing the IPOPT library [37, 38]. Two main conditions determine the convergence of the algorithm:

1. the relative tolerance on the violation of the constraints. This means that, at each step during the optimization, there is a test of the condition

$$\max_i \left| \frac{g_i - c_i}{g_i} \right| < \epsilon, \quad (20)$$

where the quantities subject to the constraints are g_i and the corresponding constraint is c_i , namely the required condition is $g_i = c_i$ within an error smaller than ϵ .

2. the tolerance on the value of the objective function f . The algorithm stops if the change in value of the objective function between two successive iterations is smaller than a given tolerance δ , namely

$$|f^{(k)} - f^{(k-1)}| < \delta, \quad (21)$$

where k is the iteration.

It is now clear that the convergence criteria for the CV and vLB methods is different. While the orthonormal condition is exactly fulfilled by the vLB method by construction, the CV method allows for some overlap of the wave functions [controlled by the quantity ϵ in Eq. (20)].

On the other side, the CV method check for the convergence of the objective function f [Eq. (21)], that is, the re-scaled radial wave functions $u_i(r)$, while the convergence criteria of the vLB method [Eq.(13)] is based on the change of the KS potential $U[\rho]$.

IV. TEST OF THE NUMERICAL METHODS

In this section, we test the two methods described in Sec. III by using target densities produced by Hartree-Fock (HF) calculations in the doubly-magic nuclei ^{40}Ca and ^{208}Pb . The benchmark HF calculations have been carried out by using the Skyrme interaction SkX [39]. Our main goals are understanding the details about the ability of the two methods to converge, and checking whether the vLB and CV methods provide consistent results when the target densities are known in very much detail and within a wide range of r . In addition, the use of theoretical HF calculations with SkX is interesting for other reasons. On the one side, the Skyrme interaction is local in space. Non-localities introduced through effective masses are very mild since, e.g., m^*/m are close to 1 in the density range spanned by protons and neutrons in ^{208}Pb , lying between 0.92 and 1 and between 1 and 1.08, respectively. As a consequence, we expect to find fairly similar SkX-HF and KS potentials.

In Fig. 1, the neutron (left) and the proton (right) target densities from the HF calculations (black solid lines) in ^{40}Ca (left) and ^{208}Pb (right) are shown. Upper panels show the different densities in a linear scale while the lower panels show the same quantities in a logarithmic scale. The logarithmic scale is important to check the asymptotics of the densities. The results of the inversion methods vLB (red dashed lines) and CV (blue dash-dotted lines) reproduce in very much detail the target HF densities. The maximum and average values (with respect to the radial coordinate) of the absolute differences are shown in Table I. In short, the reproduction of the target densities is fully satisfactory, for both neutrons and protons, with either method, in these two doubly-magic nuclei. Nevertheless, the convergence criteria in the CV method is more restrictive in these calculations, as it is evident from the same table.

The Kohn-Sham potentials obtained with the two inversion methods are shown in Fig. 2. As mentioned, the potentials are obtained up to an arbitrary constant. Such a constant should be determined such that the last occupied KS eigenvalue coincides with the HF separa-

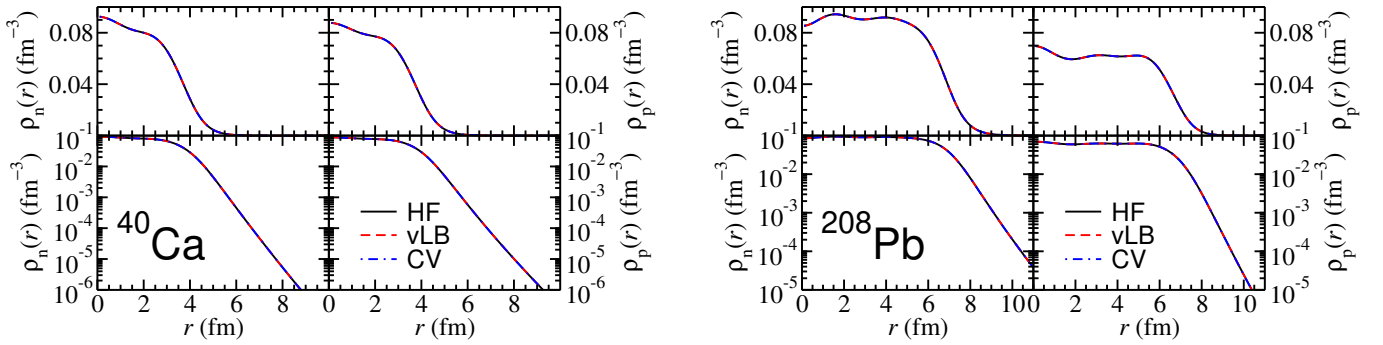


FIG. 1. Neutron density, $\rho_n(r)$, and proton density, $\rho_p(r)$, in ^{40}Ca (left panels) and ^{208}Pb (right panels), displayed as a function of the radial coordinate. In the middle panel (linear scale) and in the bottom panel (logarithmic scale) the target densities obtained from HF calculations based on the SkX functional [39] (black solid line) are compared with the densities resulting from the two inversion method that are discussed in the main text, namely vLB (red dashed line) and CV (blue dot-dashed line).

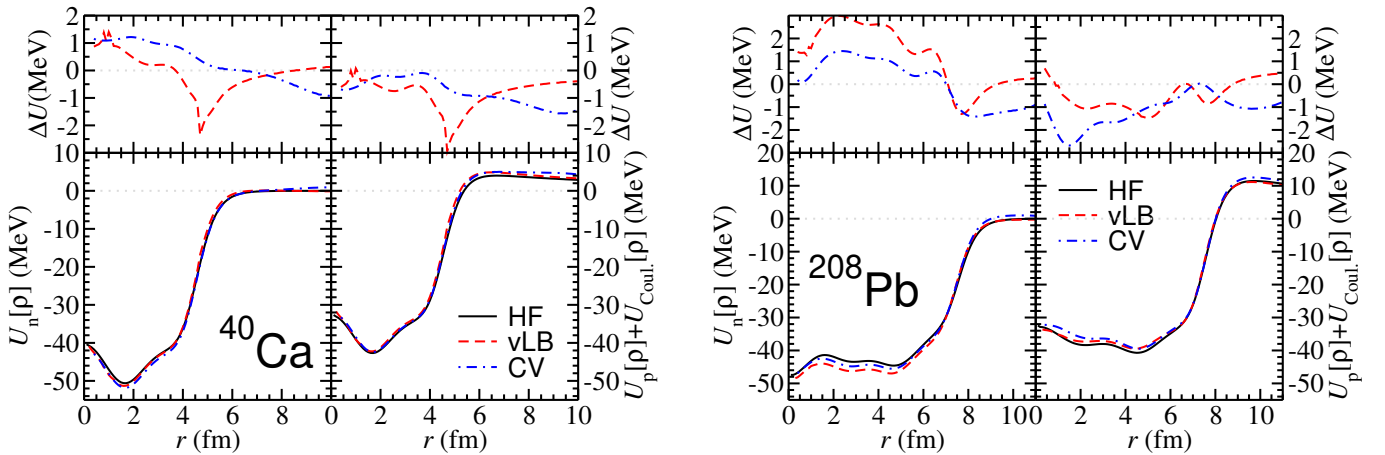


FIG. 2. The Kohn-Sham potentials obtained with the vLB (red dashed lines) and CV (blue dot-dashed lines) inversion methods in ^{40}Ca (lower left panel) and ^{208}Pb (lower right panel) are displayed as a function of the radial coordinate. The benchmark HF calculations based on the SkX functional [39] are also shown (black solid lines). In the upper panels, the differences $\Delta U \equiv U_{\text{method}} - U_{\text{HF}}$ between the vLB and CV potential and the HF potential are shown.

Nucleus	vLB		CV	
	Max.	Aver.	Max.	Aver.
^{40}Ca (p)	56.5	1.95	0.97	0.176
^{40}Ca (n)	65.7	2.17	1.03	0.186
^{208}Pb (p)	27.6	0.69	0.44	0.116
^{208}Pb (n)	55.2	4.02	7.5	2.13

TABLE I. Maximum (Max.) and average (Aver.) differences between the target HF (SkX) and KS neutron (n) and proton (p) densities from the two inversion methods for the case of ^{40}Ca and ^{208}Pb . Numerical values are all in 10^{-6} fm^{-3} .

tion energy. For simplicity, we have determined such a constant so that the last occupied KS eigenvalue coincides with the energy of the last HF occupied state. In DFT, eigenvalues and wave functions are auxiliary quantities with, strictly, no physical meaning except for the last occupied orbital that coincides with the ionization energy in atomic systems [35, 40], or neutron and pro-

ton separation energies in nuclear systems. In order to perform such a shift, we have perturbatively corrected the KS orbitals to take into account spin-orbit effects. This has allowed us to also check the reliability of our approximation in neglecting spin-orbit effects in Eq.(4). On the other side, there is another approximation since the last occupied state in a HF calculation does not exactly coincide with the HF separation energy. Hence, although the trend is correct within our numerical accuracy, this recipe for the shift produces a small deviation of the KS potentials in their asymptotic behavior [40] for $r \rightarrow \infty$. Specifically, one expects $U_n(r \rightarrow \infty) \rightarrow 0$ and $U_p + U_{\text{Coul.}}(r \rightarrow \infty) \rightarrow U_{\text{Coul.}} = \frac{(Z-1)e^2}{r}$. Nevertheless, after such a shift, the absolute value of the resulting difference ΔU with respect to the HF potentials is smaller than 2.5 MeV, both for protons and neutrons. This appears to be a quite reasonable agreement. We note that again the CV method seems to perform slightly better than the vLB method. The reason stems from the differ-

ent convergence criteria.

We now focus on the convergence of the procedures. The two algorithms behave in a quite different way. As explained in Sec. III A, the vLB method iterates the potential according to Eq. (9) and stops when the condition (13) is satisfied: in the present case, the iteration procedure is stopped when $\alpha \leq 5$ keV. In Fig. 3, we display the evolution of the potential from the vLB method (red diamonds), for the case of the neutrons in ^{208}Pb . After a transient with oscillatory behavior, namely after ≈ 500 iterations, the difference between the potentials at two different iterations goes to zero monotonically. This is visible in the linear scale of the left panel of Fig. 3, and even better in the logarithmic scale of the right panel in the same figure. Of course, the number of iterations to reach convergence depends on the value of η [cf. Eq. (10)] which is set equal to 0.01 in the present calculations.

The results from the CV method should be seen under a different light. The procedure does not use the difference between potentials at successive steps in order to proceed but rather, as explained in Sec. III B, attempts to minimize the value of the kinetic energy taking into account the tolerance with which constraints should be fulfilled. Then, the points corresponding to different iterations do not, and should not be expected to, decrease with a monotonic trend. These points (blue circles) are shown also in the two panels in Fig. 3. The convergence of the CV method shows an oscillatory behavior, which is particularly clear in the logarithmic scale of the right panel. It has to be noted that, for the sake of clarity in the presentation, only a representative point every 100 iterations is shown. With all this warnings, we can nevertheless conclude that the blue points tend to go towards smaller values as the iteration goes on and, even more importantly, they become small enough to conclude that the final result for the potential is indeed reliable.

V. RESULTS FOR EXPERIMENTAL DENSITIES

In this section, we extract different KS potentials from experimental densities [41, 42]. As case studies, we use the proton density of ^{40}Ca and the proton and neutron densities of ^{208}Pb . Specifically, the proton densities come from electron scattering data of Ref. [41] while the neutron density of ^{208}Pb has been extracted in Ref. [42]. In both references, a parameterization of the electromagnetic charge and neutron densities based on a sum of Gaussian functions (SoG) can be found. This method was first introduced in Ref. [43] to extract nuclear charge densities from elastic electron scattering data without using model distributions but a bases of well behaved functions.

The charge density distribution expressed as SoGs can

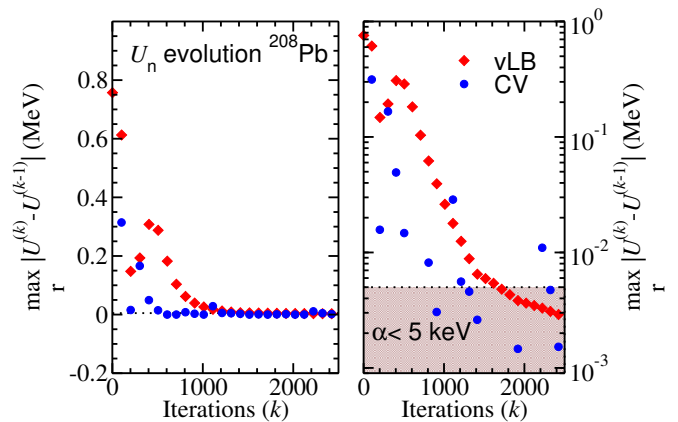


FIG. 3. Convergence test of the inversion methods, using as target density the results of a HF calculation with the SkX interaction. The absolute difference [cf. Eq. (13)] between the neutron Kohn-Sham potentials for ^{208}Pb calculated at two successive iterations are shown at different iteration steps on a linear (left panel) and on a logarithmic (right panel) scale. Results of the inversion method vLB and CV are shown by red diamonds and blue circles respectively.

be written as follows,

$$\rho_{\text{charge}}(r) = \sum_i A_i^{\text{charge}} \left(e^{-\left(\frac{r-R_i}{\gamma}\right)^2} + e^{-\left(\frac{r+R_i}{\gamma}\right)^2} \right). \quad (22)$$

The coefficients A_i^{charge} are given by

$$A_i^{\text{charge}} = \frac{ZeQ_i}{2\pi^{\frac{3}{2}}\gamma^3 \left(1 + \frac{2R_i^2}{\gamma^2}\right)}, \quad (23)$$

where Q_i is the fraction of total charge that is associated with the integral of the i -th Gaussian. Accordingly, the normalization condition $\sum_i Q_i = 1$ holds. The Gaussians are centered at different points R_i , whereas the widths are characterized by a common value γ . Sometimes, this is taken so to be close to the width of the narrowest peak that one finds when inspecting the square of typical Hartree-Fock or Woods-Saxon wave functions for the nucleus under study. The reason why the SoG parameterization (22) is chosen is that, if the sum contains enough terms, it corresponds to a model-independent representation of the actual data points. In principle, this would require a very large number of Gaussian terms if the experimental data covers the full momentum transfer range, that is from 0 to infinity. In practice this is not the case and, thus, manageable number of terms, of the order of 10-15, has been proven to be stable against small changes. As it can be easily understood, this representation may suffer from the fact that experimental data is scarce or does not cover a wide enough range for beam energies and scattering angles.

In order to extract the proton densities from the charge densities, we have neglected the small effects due to the electromagnetic spin-orbit and the neutron electromagnetic finite size (see for example Sec. II.B of Ref. [44]).

Hence, we have extracted the proton densities from the charge densities as follows,

$$\rho_{\text{charge}}(\vec{r}) = \int d^3r' f(\vec{r}') \rho_p(\vec{r} - \vec{r}'), \quad (24)$$

using the approximate electric proton form factor,

$$f(\vec{r}) = \frac{e}{\pi^{3/2}} e^{-\left(\frac{r^2}{\alpha}\right)^2}, \quad (25)$$

$$\rho_p(r) = \sum_i \frac{\gamma^3 A_i}{e\beta r} \left[\left(\frac{r - R_i}{\beta^2} + \frac{R_i}{\gamma^2} \right) e^{-\left(\frac{r-R_i}{\beta}\right)^2} + \left(\frac{r + R_i}{\beta^2} - \frac{R_i}{\gamma^2} \right) e^{-\left(\frac{r+R_i}{\beta}\right)^2} \right], \quad (26)$$

where $\beta = \sqrt{\gamma^2 - \alpha^2}$.

In the case of neutrons, such procedure is not needed as Ref. [42] provides the neutron density in the form of Eq. (22) directly. This data has been obtained via proton elastic scattering. Protons interact via the strong interaction with both, neutrons and protons. So if the proton density is known, one can derive the neutron density compatible with the experimental cross section. This procedure is not model independent contrary to the case of electron elastic scattering to determine the electromagnetic charge density.

We have implemented the same inverse problem methods and procedure described in Sec.III to the experimen-

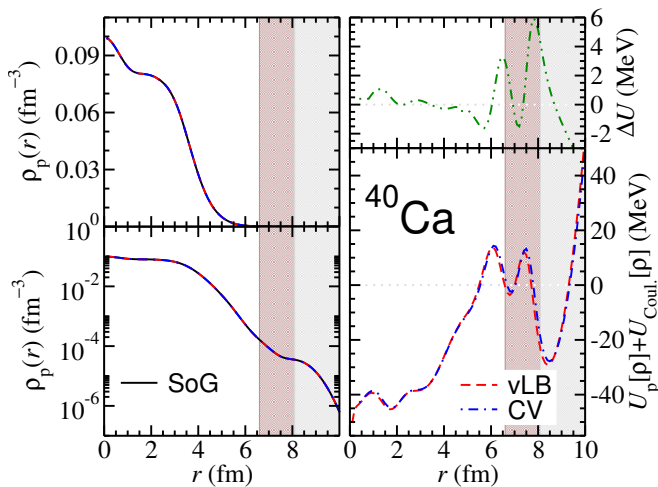


FIG. 4. The proton density for the case of ^{40}Ca is displayed as a function of the radial coordinate on a linear scale (top left panel) and on a logarithmic scale (bottom left panel). The target experimental density [41] labeled SoG –sum of Gaussians– (black solid lines) is compared with those obtained with the inversion methods vLB (red dashed lines) and CV (blue dot-dashed lines). In the bottom right panel, the Kohn-Sham potentials obtained within the two inversion methods are compared, and in the top right panel their difference $\Delta U = U_{\text{CV}} - U_{\text{vLB}}$ is shown.

tal densities and found a good agreement between those and the KS densities. The agreement can be seen in the left panels of Fig. 4 for ^{40}Ca and Fig. 5 for ^{208}Pb . The relative differences found for the densities are of the same order of those found in the previous section, although in the case of the vLB procedure for ^{40}Ca the error can reach 0.025% in the outermost region of the nucleus (cf. also Table II). Since the differences between the vLB and CV densities and the target densities are not visible in detail from the figures, the maximum and the average of the absolute value of the differences are reported in Table II.

The Kohn-Sham potentials shifted by using the experimental neutron and proton separation energies and obtained with the vLB and CV methods are also shown in Fig. 4 for ^{40}Ca and Fig. 5 for ^{208}Pb . The agreement between the two inversion methods is remarkable and of the same order of that found in Sec.IV for the test cases (see right panels in Figs. 4 and 5). However, while the potentials in the inner part of the nuclei look very reasonable, they oscillate and then tend to increase without limit in the asymptotic region. That is, the asymptotic behavior of the KS potentials at large distances is not the expected one: $U_n(r \rightarrow \infty) \rightarrow 0$ and $U_p + U_{\text{Coul.}}(r \rightarrow \infty) \rightarrow U_{\text{Coul.}} = \frac{(Z-1)e^2}{r}$. This has to be attributed to the Gaussian tail of the SoG density that both algorithms translate into a quadratic (i.e. harmonic oscillator-like) potential. To substantiate this interpretation, the regions corresponding to r larger than the radius of the outermost (second outermost) Gaussian in the case of ^{208}Pb (^{40}Ca) are shown as shadowed areas in Figs. 4 and 5, respectively. The borders of these regions are clearly correlated with the change in slope of the potentials. As a consequence, our results for the experimentally derived KS potentials cannot be regarded as reliable in the tail of the potential.

We can conclude that the employed procedure remain robust when experimental SoG densities are input and provide us with reliable information about the potential up to the average position of the nuclear surface.

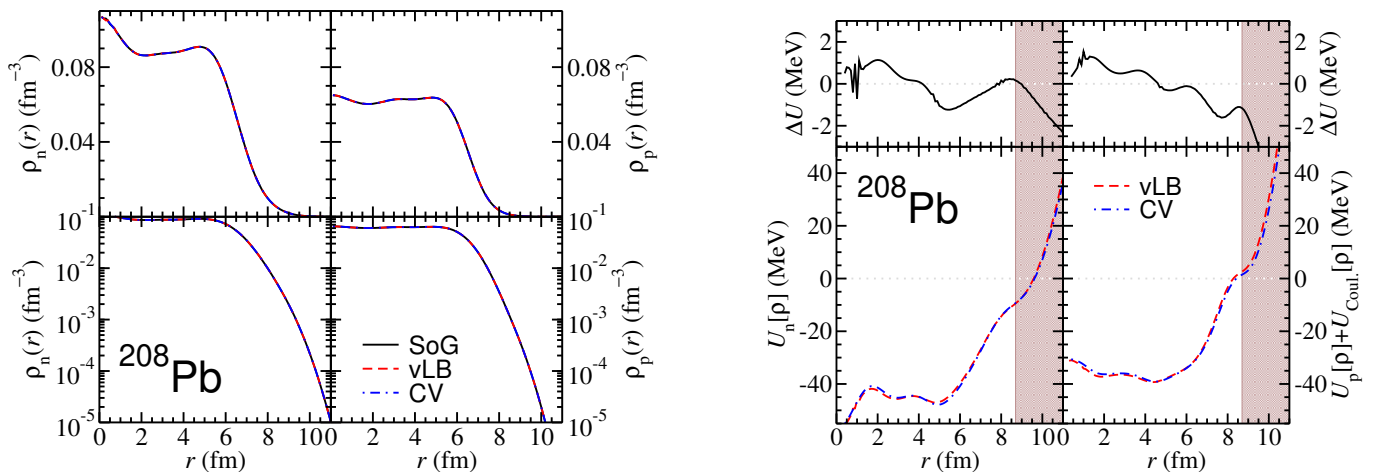


FIG. 5. (left figure) The neutron and proton densities (left panels) for the case of ^{208}Pb are displayed as a function of the radial coordinate, on a linear scale (top panels) and on a logarithmic scale (bottom panels). The target experimental densities [41] labeled as SoG –sum of Gaussians– (black solid lines) are compared with those obtained with the inversion methods vLB (red dashed lines) and CV (blue dot-dashed lines). (right figure) The Kohn-Sham potentials calculated for neutrons and protons with the inversion methods vLB (red dashed lines) and CV (blue dot-dashed lines) are shown. In the top panels, the corresponding differences between the Kohn-Sham potentials $\Delta U = U_{\text{CV}} - U_{\text{vLB}}$ are displayed.

Nucleus	vLB		CV	
	Max.	Aver.	Max.	Aver.
^{40}Ca (p)	248.	4.07	0.918	0.16
^{208}Pb (p)	8.40	0.70	0.409	0.11
^{208}Pb (n)	15.4	0.99	0.147	3.61

TABLE II. Maximum (Max.) and average (Aver.) differences between the target experimental (SoG) and KS neutron (n) and proton (p) densities from the two inversion methods for the case of ^{40}Ca and ^{208}Pb . Numerical values are all in 10^{-6} fm^{-3} .

VI. CONCLUSIONS

We have addressed, for the first time, the inverse Kohn-Sham problem applied to the atomic nucleus. Specifically, we have employed two well known inversion methods applied in other fields in physics [19]. The first method is based on an iterative procedure introduced by R. Van Leeuwen and E.J. Baerends [25] (vLB) and the second consists on a constrained minimization of the kinetic energy [19]. For our study, we restrict to closed shell spherical nuclei and use as examples ^{40}Ca and ^{208}Pb . Our first investigation has been a test of the inversion methods. For that purpose, we apply the vLB and CV methods to deduce the KS potential associated to a theoretically known density, in which the average local potential between particles is also known. The results show a remarkable agreement between either method and the benchmark calculation. These results justify the reliability of vLB and CV also when applied to the nuclear case. Hence, we have applied the inversion methods to the experimentally derived densities of protons in ^{40}Ca and ^{208}Pb and neutrons in ^{208}Pb . The results are promis-

ing and the consistency between vLB and CV remains remarkable. However, when dealing with experimental densities, one encounters some difficulties inherent to the experimental parameterizations of such densities. For the specific case of the parameterization as a sum of Gaussians (SoG) used in this work, the tails of the experimentally derived KS potentials are not reliable, opposite to what happens in the inner part and up to the average position of the nuclear surface. The fact that our results are not reliable in the tails when using a SoG is exclusively due to the non-physical Gaussian tails felt by the algorithm at large distances. Those translate into a harmonic oscillator-like potential that diverges instead of going to zero at large distances.

As our main conclusion, we have presented and validated two methods to derive the nuclear KS potential from experimental information alone. Further improvements such as the inclusion of spin-densities or spin-orbit densities should be explored. A formulation of the KS equation including these other densities as well as the important effects of the nuclear surface based on a Generalized Gradient Approximation such in other fields in physics should be pursued. Ultimately, the derivation of the nuclear EDF from the KS potential may require the use of theoretical benchmarks. This line of research is unexplored.

ACKNOWLEDGMENTS

Funding from the European Union’s Horizon 2020 research and innovation programme under grant agreement No 654002 is acknowledged.

-
- [1] M. Bender, P.-H. Heenen, and P.-G. Reinhard, *Rev. Mod. Phys.* **75**, 121 (2003).
- [2] N. Schunck, ed., *Energy Density Functional Methods for Atomic Nuclei*, 2053-2563 (IOP Publishing, 2019).
- [3] K. Burke, *The Journal of Chemical Physics* **136**, 150901 (2012), <https://doi.org/10.1063/1.4704546>.
- [4] A. D. Becke, *The Journal of Chemical Physics* **140**, 18A301 (2014).
- [5] P. Hohenberg and W. Kohn, *Phys. Rev.* **136**, B864 (1964).
- [6] F. Raimondi, B. G. Carlsson, and J. Dobaczewski, *Phys. Rev. C* **83**, 054311 (2011).
- [7] P. Becker, D. Davesne, J. Meyer, J. Navarro, and A. Pastore, *Phys. Rev. C* **96**, 044330 (2017).
- [8] Y. Engel, D. Brink, K. Goeke, S. Krieger, and D. Vautherin, *Nuclear Physics A* **249**, 215 (1975).
- [9] J. Dobaczewski and J. Dudek, *Acta Physica Polonica B* **27**, 45 (1996).
- [10] E. Perlińska, S. G. Rohoziński, J. Dobaczewski, and W. Nazarewicz, *Phys. Rev. C* **69**, 014316 (2004).
- [11] J. Drut, R. Furnstahl, and L. Platter, *Progress in Particle and Nuclear Physics* **64**, 120 (2010).
- [12] L. G. Cao, U. Lombardo, C. W. Shen, and N. V. Giai, *Phys. Rev. C* **73**, 014313 (2006).
- [13] M. Baldo, P. Schuck, and X. Vias, *Physics Letters B* **663**, 390 (2008).
- [14] D. Gambacurta, L. Li, G. Colò, U. Lombardo, N. Van Giai, and W. Zuo, *Phys. Rev. C* **84**, 024301 (2011).
- [15] M. Stoitsov, M. Kortelainen, S. K. Bogner, T. Duguet, R. J. Furnstahl, B. Gebremariam, and N. Schunck, *Phys. Rev. C* **82**, 054307 (2010).
- [16] S. K. Bogner, R. J. Furnstahl, H. Hergert, M. Kortelainen, P. Maris, M. Stoitsov, and J. P. Vary, *Phys. Rev. C* **84**, 044306 (2011).
- [17] R. Navarro Pérez, N. Schunck, A. Dyhdalo, R. J. Furnstahl, and S. K. Bogner, *Phys. Rev. C* **97**, 054304 (2018).
- [18] W. Kohn and L. J. Sham, *Phys. Rev.* **140**, A1133 (1965).
- [19] D. S. Jensen and A. Wasserman, *International Journal of Quantum Chemistry* **118**, e25425 (2018).
- [20] J. Engel, *Phys. Rev. C* **75**, 014306 (2007).
- [21] K. Capelle, *The Journal of Chemical Physics* **119**, 1285 (2003), <https://doi.org/10.1063/1.1593014>.
- [22] N. Barnea, *Phys. Rev. C* **76**, 067302 (2007).
- [23] J. Messud, M. Bender, and E. Suraud, *Phys. Rev. C* **80**, 054314 (2009).
- [24] Y. Wang and R. G. Parr, *Phys. Rev. A* **47**, R1591 (1993).
- [25] R. van Leeuwen and E. J. Baerends, *Phys. Rev. A* **49**, 2421 (1994).
- [26] E. A. Hylleraas, *Zeitschrift für Physik* **54**, 347 (1929).
- [27] J. Li, N. D. Drummond, P. Schuck, and V. Olevano, *SciPost Phys.* **6**, 40 (2019).
- [28] S. E. B. Nielsen, M. Ruggenthaler, and R. van Leeuwen, *EPL (Europhysics Letters)* **101**, 33001 (2013).
- [29] S. E. B. Nielsen, M. Ruggenthaler, and R. van Leeuwen, *The European Physical Journal B* **91**, 235 (2018).
- [30] A. Kumar, R. Singh, and M. K. Harbola, *Journal of Physics B: Atomic, Molecular and Optical Physics* **52**, 075007 (2019).
- [31] J. Hadamard, *Princeton Univ. Bull.* **13**, 49 (1902).
- [32] J. T. Chayes, L. Chayes, and M. B. Ruskai, *Journal of Statistical Physics* **38**, 497 (1985).
- [33] E. Engel and R. Dreizler, “Density functional theory,” (Springer, 2011).
- [34] J. Dobaczewski, *Journal of Physics G: Nuclear and Particle Physics* **43**, 04LT01 (2016).
- [35] J. P. Perdew, R. G. Parr, M. Levy, and J. L. Balduz, *Phys. Rev. Lett.* **49**, 1691 (1982).
- [36] Q. Wu and W. Yang, *The Journal of Chemical Physics* **118**, 2498 (2003).
- [37] A. Wächter and L. T. Biegler, *Mathematical Programming* **106**, 25 (2006).
- [38] A. Wächter, “Short tutorial: Getting started with ipopt in 90 minutes,” In H. D. Simon U. Naumann, O. Schenk, editor, *Combinatorial Scientific Computing*. 2009.
- [39] B. Alex Brown, *Phys. Rev. C* **58**, 220 (1998).
- [40] J. P. Perdew and M. Levy, *Phys. Rev. B* **56**, 16021 (1997).
- [41] H. D. Vries, C. D. Jager, and C. D. Vries, *Atomic Data and Nuclear Data Tables* **36**, 495 (1987).
- [42] J. Zenihiro, H. Sakaguchi, T. Murakami, M. Yosoi, Y. Yasuda, S. Terashima, Y. Iwao, H. Takeda, M. Itoh, H. P. Yoshida, and M. Uchida, *Phys. Rev. C* **82**, 044611 (2010).
- [43] I. Sick, *Nuclear Physics A* **218**, 509 (1974).
- [44] L. Ray, *Phys. Rev. C* **19**, 1855 (1979).